Chaos, Solitons and Fractals 199 (2025) 116870

Contents lists available at ScienceDirect

Chaos, Solitons and Fractals

journal homepage: www.elsevier.com/locate/chaos

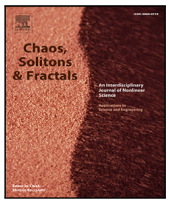

Contribution of the 2021 COVID-19 vaccination regime to COVID-19 transmission and control in South Africa: *A mathematical modeling perspective*

Tesfalem A. Tegegn [a], Yibeltal A. Terefe [b,*]

[a] Department of Mathematics and Applied Mathematics University of Pretoria, Private bag X20 Hatfield, Pretoria, 0028, Gauteng, South Africa
[b] Department of Mathematics and Applied Mathematics University of the Free State, P.O. Box 339, Bloemfontein, 9300, Free State, South Africa

ARTICLE INFO

Dataset link: https://github.com/CSSEGISandData/COVID-19

MSC:
34A34
37N25
65L12
65L99
92B05
92D30

Keywords:
COVID-19
Vaccines
Basic reproduction number
Stability
Sensitivity analysis

ABSTRACT

This study assesses the impact of COVID-19 vaccines through an epidemiological model that quantifies their role in pandemic control. We analyze an SIR-based model incorporating vaccination effects and calculate the basic reproduction number, $\mathcal{R}_0$. Our findings indicate that under conditions of imperfect vaccination and non-permanent immunity from recovery, a backward bifurcation may occur when $\mathcal{R}_0 < 1$. Conversely, with full immunity from vaccination and lasting immunity post-recovery, the disease-free equilibrium is globally asymptotically stable for $\mathcal{R}_0 < 1$. Numerical simulations support these theoretical results. The model is calibrated using South African data from Johns Hopkins University, covering the period from February 17 to August 5, 2021. Results show that vaccine effectiveness in preventing infection was below 50%, consistent with the CDC's February 2024 report indicating an improved infection-protection rate of 54% for newly produced vaccines. Additionally, our findings demonstrate that vaccines significantly enhanced recovery rates and reduced both mortality and recovery time, aligning with CDC reports. A sensitivity analysis highlights key parameters affecting $\mathcal{R}_0$, offering insights for policymakers on optimizing vaccination strategies.

1. Introduction

COVID-19 is an infectious disease caused by SARS-CoV-2 virus, which prompted the World Health Organization (WHO) to declare Public Health Emergency of International Concern on 30 January 2020, and latter a pandemic on 11 March 2020. First detected in December 2019 in Wuhan, China, the virus has since spread to all seven continents and every country recognized by the United Nations as a sovereign state. According to the worldometers database[1], COVID-19 infected well over 700 million people and claimed over 7 million lives as of 24 July 2024.

Measures implemented to curb the spread of COVID-19 including large-scale lockdowns, social distancing and others, significantly disrupted family and social life while badly affecting the global economy by crippling global and local supply chains [2–8]. Global financial institutions, including the World Bank and International Monetary Fund (IMF), repeatedly revised their projections for global economic growth during the pandemic. A McKinsey & Company report (October 2021) [9] highlighted the COVID-19 related concerns, particularly travel restrictions and supply chain disruption, were perceived by both corporate leaders and government officials as the most significant threats to domestic and corporate economic growth.

The SARS-CoV-2 virus primarily spreads from person to person through small respiratory droplets, known as aerosols, which are released when an infected individual coughs, sneezes, talks, or engages in similar activities [10]. Initially, due to the relatively large size of the virus, it was assumed that transmission could occur only via larger droplets, which were believed to remain airborne for only a short time and to travel no more than two meters from the source. However, Van Doremalen et al. [11] demonstrated that SARS-CoV-2 can remain airborne for at least three hours, with a viral load sufficient to cause infection. This finding indicates that the virus is indeed airborne, helping to explain its rapid spread and the limited effectiveness of control measures such as lockdowns and social distancing. Another significant mode of transmission is through contact with contaminated surfaces, such as doorknobs, stair railings, and elevator buttons, followed by touching the nose, mouth, or eyes before hand hygiene. Studies have shown that the virus can remain viable on hard surfaces for varying durations depending on the material [11].

* Corresponding author.
E-mail address: yibadan@gmail.com (Y.A. Terefe).

https://doi.org/10.1016/j.chaos.2025.116870
Received 15 November 2024; Received in revised form 14 June 2025; Accepted 7 July 2025
Available online 22 July 2025

Since the end of the 18th century, mathematical models have been in use in public health areas and have provided useful information for policy makers. These models also assist public health professionals by generating valuable information to design mitigation and control strategies, see [12]. In the context of COVID-19 pandemic, several mathematical models have been proposed and analyzed to understand the transmission dynamics of the disease. One of the earliest works in this regard is [13] in which the authors used a simple SEIR model to estimate the pandemics trajectory. Subsequent studies, such as [14] proposed a modified SIR model to analyze the role of environmental contamination by infected individuals. In [15], an SIR-based model was proposed to assess the effectiveness of mitigation strategies recommended by the WHO. Similarly, [16] proposed SEIR-based model to analyze the impact of cross-boarder migration, with and without screening at boarder crossings, on disease prevalence in the host community. Indeed, in the context of pandemics, one of the key contributions of mathematical research is to project the epidemic trajectory and recommend effective control mechanisms to support public health policy decisions.

Vaccines have long played a crucial role in controlling pandemics such as smallpox, yellow fever, and influenza. Although vaccines do not offer 100% protection, they significantly reduce the risk of infection, severe illness, and death. In the case of COVID-19, it is well established that the efficacy[1] of vaccines is high for a limited period. They have been shown to be particularly effective in preventing severe illness, reducing the risk of infection, and lowering mortality associated with the virus. Despite not being perfect, widespread vaccination campaigns were carried out globally, and they played a critical role in bringing the COVID-19 pandemic under control.

The primary objective of this study is not to nowcast or forecast the trajectory of the COVID-19 outbreak, but rather to assess the contribution of vaccines administered in South Africa during the period 17 March to 5 August 2021. The specific time frame was chosen solely based on data availability; a detailed explanation is provided in Section 4.1. To achieve this goal, we propose an SIRS-based epidemiological model in which the susceptible population is divided into vaccinated and unvaccinated classes based on their vulnerability. A vaccinated individual is defined as someone who has received at least one dose of any vaccine legally approved and administered in the country. The model accounts for important real-world considerations, including the fact that vaccines do not offer complete protection and reinfection is possible. The model also considers separate compartments for infectious people from the two susceptible groups so as to be able to analyze how vaccines helped the infected to recover. Additionally, separate compartments are included for infectious individuals originating from both susceptible groups, enabling a detailed analysis of how vaccination influences recovery outcomes. Overall, this study introduces a novel epidemic model that classifies infected individuals into vaccinated and unvaccinated subgroups, further stratified by symptomatic and asymptomatic status. This structure enables a targeted evaluation of vaccine efficacy in facilitating recovery, an aspect that is not commonly addressed in existing literature. The full model formulation and associated assumptions are presented in Section 2.

Section 3 is dedicated to the qualitative and quantitative analysis of the proposed model. In this section, we compute the basic reproduction number, identify the disease-free and endemic equilibrium points, and analyze their stability, among other aspects. For the numerical analysis, we used Python libraries such as Pandas, NumPy, lmfit, and others to download data from [17], preprocess it, fit it to the model, and perform local sensitivity analysis. A comprehensive discussion on the data, primary parameter estimation, model fitting, sensitivity analysis, and interpretation of the results is presented in Sections 4, 5, and 6, respectively.

[1] According to the World Health Organization [10], vaccine efficacy refers to how well a vaccine prevents disease under ideal, controlled clinical trial conditions, whereas vaccine effectiveness describes how well it performs in real-world settings.

2. Model formulation

In this section, we propose a mathematical model designed to capture the contribution of vaccines in two key aspects: reducing the risk of infection, and, in cases where infection occurs despite vaccination, mitigating symptoms and enhancing the recovery rate.

To formulate the model, we begin by assuming that the population is mixed homogeneously. Based on individuals' vulnerability to infection and infection status, the total population is divided into eight mutually exclusive compartments. Susceptible individuals who have not received COVID-19 vaccines are placed in S class. Those who have received at least one dose of any approved COVID-19 vaccine are assigned to the V class. Unvaccinated individuals who become infected are classified as either symptomatic (I) or asymptomatic (A). In cases where vaccination does not prevent infection, vaccinated individuals may still become infected and are classified as asymptomatic (A_1) or symptomatic (I_1). Infectious individuals who are isolated, whether in hospitals or temporary treatment centers or own facilities, are placed in the Q class. Finally, individuals who have recovered from COVID-19 are assigned to the R class.

Thus, the total population at time t, denoted by $N(t)$, is given by

$$N(t) = S(t) + V(t) + A(t) + A_1(t) + I(t) + I_1(t) + Q(t) + R(t), \tag{1}$$

where $S(t)$, $V(t)$, $A(t)$ $A_1(t)$, $I(t)$, $I_1(t)$, $Q(t)$ and $R(t)$ represent the number of individuals in compartments S, V, A, A_1, I, I_1, Q and R, respectively, at time t. For convenience, we will hereafter refer to these variables as S, V, A, A_1, I, I_1, Q, and R instead of explicitly writing them as functions of time, unless otherwise necessary.

In formulating the model, we excluded both the exposed (latent) compartment and the contribution of environmental contamination in order to facilitate a more tractable mathematical analysis. More specifically, although COVID-19 is known to transmit through both direct human-to-human contact and indirect contact via contaminated surfaces, this model considers only direct transmission. That is, we focus on transmissions arising from interactions between susceptible individuals and infectious individuals, such as through inhalation of virus laden aerosols or physical contacts, such as handshake.

Given that the model includes four classes of infectious individuals, namely, symptomatic unvaccinated (I), asymptomatic unvaccinated (A), symptomatic vaccinated (I_1), and asymptomatic vaccinated (A_1) who may interact with the susceptible individuals, we define the force of infection as:

$$\lambda = \beta \frac{I + \nu A + \nu_1 A_1 + \kappa I_1}{N}, \tag{2}$$

where β denotes the transmission rate, and ν, ν_1 and κ are modification parameters that account for the relative infectiousness of compartments A, A_1, and I_1, respectively, compared to the symptomatic unvaccinated class I. Individuals in the isolated compartment Q are assumed not to contribute to disease transmission, as they are separated from the susceptible population.

Apart from the assumption of homogeneous mixing of the population the model is designed based on the following main assumptions:

(1) Individuals who recover from COVID–19 acquire temporary immunity and eventually return to the susceptible class after the immunity wanes.
(2) The severity of disease and COVID-19-induced mortality differ based on vaccination status. Specifically, δ denotes the disease-induced death rate for unvaccinated individuals, while δ_1 represents the corresponding rate for vaccinated individuals.
(3) Disease transmission is primarily driven by interactions between infectious and susceptible individuals. Consequently, the force of infection λ is formulated in terms of the infectious compartments and their respective contact rates with susceptibles.
(4) A constant recruitment rate Λ (due to births and migration) is assumed into the susceptible class S. During lockdown periods, Λ is primarily attributable to natural births.

Based on these assumptions outlined above, we now formulate the system of differential equations governing the dynamics of each compartment. In particular, Eqs. (3) and (4) describe the evolution of susceptible unvaccinated (S) and vaccinated (V) populations, respectively:

$$S'(t) = \Lambda - [\lambda + (\sigma + \mu)]S + \varphi R, \tag{3}$$

$$V'(t) = \sigma S - [(1-\rho)\lambda + \mu]V + (\omega - \varphi)R. \tag{4}$$

Here, Λ denotes the recruitment rate into the S class, which may result from births and migration. The parameter σ represents rate at which susceptible individuals are vaccinated, while μ is the natural death rate. The vaccine effectiveness is denoted by ρ, indicating the degree to which vaccination reduces susceptibility to infection. The parameter ω captures the overall rate at which individuals exit the R class, and φ accounts for the fraction of recovered individuals who lose their temporary immunity and either refuse vaccination or lack access to it.

The dynamics of infectious classes A, I, A_1 and I_1 are described by the system of Eqs. (5)–(8):

$$A'(t) = \eta\lambda S - (\mu + \theta + \gamma_1)A, \tag{5}$$

$$I'(t) = (1-\eta)\lambda S - (\epsilon + \gamma_2 + \delta + \mu)I, \tag{6}$$

$$A_1'(t) = \phi(1-\rho)\lambda V - (\theta_1 + \gamma_4 + \mu)A_1, \tag{7}$$

$$I_1'(t) = (1-\phi)(1-\rho)\lambda V - (\epsilon_1 + \gamma_5 + \delta_1 + \mu)I_1, \tag{8}$$

In this system, η denotes the proportion of unvaccinated individuals who become asymptomatic upon infection, while ϕ represents the corresponding proportion among vaccinated individuals. The parameters θ and γ_1 are the isolation/quarantine and recovery rates, respectively, for the unvaccinated asymptomatic class A; and θ_1 and γ_4 are the their counterparts for the vaccinated asymptomatic class A_1. For the symptomatic classes, ϵ and ϵ_1 denote isolation rates, γ_2 and γ_5 are recovery rates, and δ and δ_1 are COVID-19-induced mortality rates for the unvaccinated I and vaccinated I_1 compartments, respectively.

The dynamics of the quarantine/isolation compartment Q and recovered compartment R are governed by equations:

$$Q'(t) = \theta A + \epsilon I + \theta_1 A_1 + \epsilon_1 I_1 - (\gamma_3 + \delta + \mu)Q, \tag{9}$$

$$R'(t) = \gamma_1 A + \gamma_2 I + \gamma_3 Q + \gamma_4 A_1 + \gamma_5 I_1 - (\omega + \mu)R. \tag{10}$$

Here, γ_3 represents the recovery rate from the isolation compartment Q to the recovered compartment R. The complete transmission dynamics of the disease in the population is illustrated in Fig. 1 and a summary description of the model's state variables and parameters is presented in Table 1.

Collecting Eqs. (3)–(10), we arrive at the following system of nonlinear ordinary differential equations governing the model dynamics:

$$S'(t) = \Lambda - [\lambda + \sigma + \mu]S + \varphi R, \tag{11a}$$

$$V'(t) = \sigma S - [(1-\rho)\lambda + \mu]V + (\omega - \varphi)R, \tag{11b}$$

$$A'(t) = \eta\lambda S - (\theta + \gamma_1 + \mu)A, \tag{11c}$$

$$I'(t) = (1-\eta)\lambda S - (\epsilon + \delta + \gamma_2 + \mu)I, \tag{11d}$$

$$A_1'(t) = \phi(1-\rho)\lambda V - (\theta_1 + \gamma_4 + \mu)A_1, \tag{11e}$$

$$I_1'(t) = (1-\phi)(1-\rho)\lambda V - (\epsilon_1 + \gamma_5 + \delta_1 + \mu)I_1, \tag{11f}$$

$$Q'(t) = \theta A + \theta_1 A_1 + \epsilon I + \epsilon_1 I_1 - (\gamma_3 + \delta + \mu)Q, \tag{11g}$$

$$R'(t) = \gamma_1 A + \gamma_2 I + \gamma_3 Q + \gamma_4 A_1 + \gamma_5 I_1 - (\omega + \mu)R. \tag{11h}$$

The system (11) is equipped with non-negative initial conditions:

$$S(0) = S_0,\ V(0) = V_0,\ A(0) = A_0,\ I(0) = I_0,\ Q(0) = Q_0,\ \text{and}\ \ R(0) = R_0. \tag{12}$$

The next section is devoted to the analysis of model (11) together with the initial conditions in (12).

3. Quantitative and qualitative analysis

A critical first step in analyzing model (11) is demonstrating its epidemiological feasibility, such as ensuring solutions remain biologically meaningful (e.g., non-negative and bounded). We formalize this property in Theorem 3.1, with the full proof provided in Appendix A. The proof primarily employs the method of contradiction, following the approach in [18,19], to establish non-negativity. Boundedness is demonstrated using Gronwall's lemma, while uniqueness follows directly from Theorem 2.1.5 in [20].

Theorem 3.1. *The model (11) is a dynamical system on the region*

$$\Omega = \left\{ (S,V,A,I,A_1,I_1,Q,R) \in \mathbb{R}_+^8 : 0 \le S+V+A+A_1+I+I_1+Q+R = N \le \frac{\Lambda}{\mu} \right\}, \tag{13}$$

where $\mathbb{R}_+^8$ denotes the portion of $\mathbb{R}^8$ with all its components non-negative.

Having established the feasibility of the system (11)–(12), we proceed to derive its equilibrium points and analyze their stability. The equilibria are obtained by setting the right-hand side of (11) to zero. In particular, by setting all infected compartments to zero, we obtain the trivial equilibrium, denoted by E_0, which represents the disease-free equilibrium (DFE) given by (14):

$$E_0 = (S,V,A,I,A_1,I_1,Q,R) = \left(\frac{\Lambda}{\sigma+\mu}, \frac{\sigma\Lambda}{\mu(\sigma+\mu)}, 0,0,0,0,0,0\right). \tag{14}$$

If a non-trivial equilibrium solution E^* exists, where at least one infected compartment is non-zero, it is referred to as an endemic equilibrium. We denote this equilibrium as

$$E^* = (S^*, V^*, A^*, I^*, A_1^*, I_1^*, Q^*, R^*) \tag{15}$$

representing persistence infection within the population, even when the system is at equilibrium. We analyze the existence and stability of E^* for the system (11) in Section 3.1.

To analyze the stability of the equilibrium points, we compute the threshold parameter known as the basic reproduction number, denoted by $\mathcal{R}_0$. Using the Next Generation Matrix (NGM) method as in [21–24] we obtain

$$\mathcal{R}_0 = \mathcal{R}_A + \mathcal{R}_I + \mathcal{R}_{A_1} + \mathcal{R}_{I_1}, \tag{16}$$

where

$$\mathcal{R}_A = \frac{\nu B_1}{k_1},\ \mathcal{R}_I = \frac{B_2}{k_2},\ \mathcal{R}_{A_1} = \frac{\nu_1 B_3}{k_3},\ \mathcal{R}_{I_1} = \frac{\kappa B_4}{k_4},$$

and B_i and k_i for $i = 1, 2, 3, 4$ are defined as

$$B_1 = \frac{\eta\beta\mu}{\sigma+\mu},\ B_2 = \frac{(1-\eta)\beta\mu}{\sigma+\mu},\ B_3 = \frac{\phi(1-\rho)\beta\sigma}{\sigma+\mu},\ B_4 = \frac{(1-\phi)(1-\rho)\beta\sigma}{\sigma+\mu},$$

$$k_1 = \theta + \gamma_1 + \mu,\ k_2 = \epsilon + \gamma_2 + \delta + \mu,\ k_3 = \theta_1 + \gamma_4 + \mu,$$

$$k_4 = \epsilon_1 + \gamma_5 + \delta_1 + \mu.$$

A detailed derivation of $\mathcal{R}_0$ is provided in Appendix B.

Remark 3.2. In (16), the terms $\mathcal{R}_A$, $\mathcal{R}_I$, $\mathcal{R}_{A_1}$ and $\mathcal{R}_{I_1}$ represent the respective contributions of the four infectious compartments A, I, A_1 and I_1 to the overall transmission potential of the diseases.

Remark 3.3. When both vaccination and recovery confer permanent immunity (i.e., $\rho = 1$ and $\omega = 0$), the basic reproduction number in (16) simplifies to

$$\mathcal{R}_0 = \mathcal{R}_A + \mathcal{R}_I, \tag{17}$$

indicating that only the unvaccinated infectious compartments contribute to disease transmission under this assumption.

The local asymptotic stability of the disease free equilibrium E_0, as stated in Theorem 3.4, follows directly from Theorem 2 of [23].

Theorem 3.4. *The disease-free equilibrium, E_0 of the model (11) is locally asymptotically stable if $\mathcal{R}_0 < 1$ and unstable whenever $\mathcal{R}_0 > 1$.*

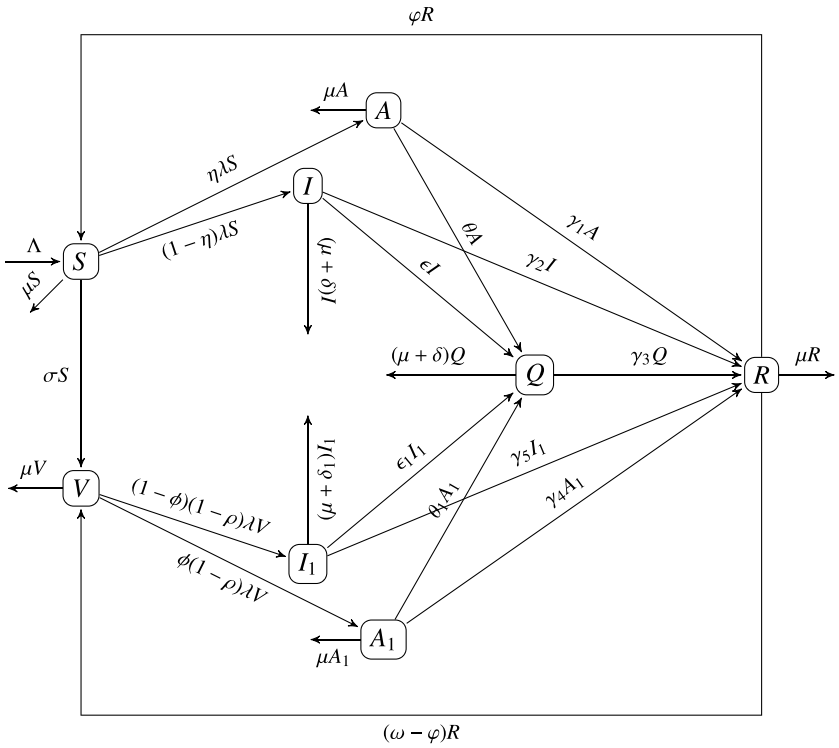

Fig. 1. The schematic diagram for model (11).

Table 1
Description of variables and parameters of model (11).

Variable	Description
S	Susceptible class
V	Vaccinated class
A	Asymptomatic and not vaccinated class
A_1	Asymptomatic but vaccinated class
I	symptomatic and not vaccinated class
I_1	Symptomatic but vaccinated class
Q	A class containing hospitalized individuals
R	Recovered class
Parameter	**Description**
Λ	Recruitment rate for S class
σ	Rate of vaccination
μ	Natural death rate
θ	Rate of quarantine from class A
θ_1	Rate of quarantine from class A_1
γ_1, γ_2, γ_3, γ_4, γ_5	Rates of transfer from A, I, Q, A_1 and I_1 classes, respectively to R class
ω	Rate of losing immunity from R class
φ	Fraction of recovered individuals who lost immunity but not vaccinated
ρ	Vaccine effectiveness
η	Fraction of infected individuals who remain asymptomatic
ϕ	Fraction of infected but vaccinated individuals who remain asymptomatic
ϵ	Rate of isolation from I class
ϵ_1	Rate of isolation from I_1 class
δ	Death rate due to COVID-19 for I and Q classes
δ_1	Death rate due to COVID-19 for I_1 class
β	Effective contact rate in the community
ν, ν_1, κ	Modification parameters

3.1. Existence of backward bifurcation

The epidemiological implication of Theorem 3.4 is that when $\mathcal{R}_0 < 1$, a small influx of infected individuals into the community will not trigger an outbreak, and the disease eventually dies out. However, for disease elimination to be guaranteed regardless of the initial conditions, it is necessary to show that the disease-free equilibrium (E_0) is globally asymptotically stable when $\mathcal{R}_0 < 1$. If the model exhibits a backward bifurcation, then the disease may persist in the population even when $\mathcal{R}_0 < 1$, thereby undermining this threshold behavior associated with the basic reproduction number.

To investigate the possibility of a backward bifurcation in the model, we examine the existence of a non-trivial endemic equilibrium $E^* = \left(S^*, V^*, A^*, I^*, A_1^*, I_1^*, Q^*, R^*\right)$ under the condition $\mathcal{R}_0 < 1$. This equilibrium satisfies the system of Eqs. (18):

$$
\begin{aligned}
&\Lambda - [\lambda^* + \sigma + \mu]S^* + \varphi R^* = 0,\\
&\sigma S^* - [(1-\rho)\lambda^* + \mu]V^* + (\omega - \varphi)R^* = 0,\\
&\eta\lambda^* S^* - k_1 A^* = 0,\\
&(1-\eta)\lambda^* S^* - k_2 I^* = 0,\\
&\phi(1-\rho)\lambda^* V^* - k_3 A_1^* = 0,\\
&(1-\phi)(1-\rho)\lambda^* V^* - k_4 I_1^* = 0,\\
&\theta A^* + \theta_1 A_1^* + \epsilon I^* + \epsilon_1 I_1^* - k_5 Q^* = 0,\\
&\gamma_1 A^* + \gamma_2 I^* + \gamma_3 Q^* + \gamma_4 A_1^* + \gamma_5 I_1^* - (\omega + \mu)R^* = 0,
\end{aligned}
\tag{18}
$$

where

$$
\lambda^* = \beta \frac{I^* + \nu A^* + \nu_1 A_1^* + \kappa I_1^*}{N^*} \tag{19}
$$

is the force of infection and

$$
N^* = S^* + V^* + A^* + I^* + A_1^* + I_1^* + Q^* + R^*, \tag{20}
$$

the total population at the equilibrium.

While solving the full system (18) is analytically challenging, each equilibrium compartment, namely A^*, I^*, A_1^*, I_1^*, Q^*, R^*, S^* and V^*, can be expressed explicitly in terms of λ^* as follows:

$$
\begin{aligned}
&A^* = \frac{\eta\lambda^* S^*}{k_1}, \quad A_1^* = \frac{\phi(1-\rho)\lambda^* V^*}{k_3}, \quad I_1^* = \frac{(1-\phi)(1-\rho)\lambda^* V^*}{k_4},\\
&Q^* = \frac{\lambda^*}{k_5}\left(t_1 S^* + t_2 V^*\right), \quad R^* = \frac{\lambda^*}{\omega + \mu}\left(t_3 S^* + t_4 V^*\right),\\
&I^* = \frac{(1-\eta)\lambda^* S^*}{k_2}\\
&S^* = t_5 V^* + t_6, \quad \text{and} \quad V^* = \frac{(\sigma + x t_3 \lambda^*)t_6}{(1-\rho)\lambda^* + \mu - (\sigma t_5 + x\lambda^*(t_3 t_5 + t_4))}
\end{aligned}
\tag{21}
$$

where

$$
\begin{aligned}
&k_5 = \gamma_3 + \delta + \mu, \quad t_1 = \frac{\eta\theta}{k_1} + \frac{\epsilon(1-\eta)}{k_2},\\
&t_2 = \frac{\phi(1-\rho)\theta_1}{k_3} + \frac{\epsilon_1(1-\phi)(1-\rho)}{k_4},\\
&t_3 = \frac{\gamma_1\eta}{k_1} + \frac{\eta_2(1-\eta)}{k_2} + \frac{\gamma_3 t_1}{k_5}, \quad t_4 = \frac{\gamma_3 t_2}{k_5} + \frac{\gamma_4\phi(1-\rho)}{k_3} + \frac{\gamma_5(1-\phi)(1-\rho)}{k_4},\\
&t_5 = \frac{\varphi t_4}{(\omega+\mu)(\lambda^* + \sigma + \mu) - \varphi\lambda^* t_3}, \quad t_6 = \frac{(\omega+\mu)\Lambda}{(\omega+\mu)(\lambda^* + \sigma + \mu) - \varphi\lambda^* t_3},\\
&x = \frac{\omega - \varphi}{\omega + \mu}.
\end{aligned}
$$

Through algebraic manipulation of Eqs. (19), (20), and (21), we obtain a polynomial of degree four in λ^* of the form:

$$
H(\lambda^*) = \lambda^* P(\lambda^*), \tag{22}
$$

where

$$
P(\lambda^*) = Q_3(\lambda^*)^3 + Q_2(\lambda^*)^2 + Q_1\lambda^* + Q_0, \tag{23}
$$

and

$$
\begin{aligned}
Q_3 &= F_3(\omega + \mu - \varphi t_3) > 0,\\
Q_2 &= F_3(\omega+\mu)(\sigma+\mu) + F_2(\omega + \mu - \varphi t_3),\\
Q_1 &= F_2(\omega+\mu)(\sigma+\mu) + F_1(\omega + \mu - \varphi t_3),\\
Q_0 &= F_1(\omega+\mu)(\sigma+\mu) = (\omega+\mu)(\sigma+\mu)^2(1 - \mathcal{R}_0).
\end{aligned}
\tag{24}
$$

The auxiliary terms F_1, F_2, F_3 are defined as:

$$
\begin{aligned}
F_1 &= \sigma D_1 + \mu D_3,\\
F_2 &= D_1 t_3 x + \sigma D_2 + \left(1 - \rho - t_4 x\right) D_3 + \mu D_4,\\
F_3 &= D_2 t_3 x + \left(1 - \rho - t_4 x\right) D_4,
\end{aligned}
$$

with the intermediate coefficients D_1, D_2, D_3, D_4 given by:

$$
\begin{aligned}
D_1 &= 1 - \left(\frac{\nu_1\phi(1-\rho)\beta}{k_3} + \frac{\kappa(1-\phi)(1-\rho)\beta}{k_4}\right),\\
D_2 &= \frac{\phi(1-\rho)}{k_3} + \frac{(1-\phi)(1-\rho)}{k_4} + \frac{t_2}{k_5} + \frac{t_4}{\omega+\mu},\\
D_3 &= 1 - \left(\frac{\nu\eta\beta}{k_1} + \frac{(1-\eta)\beta}{k_2}\right),\\
D_4 &= \frac{\eta}{k_1} + \frac{(1-\eta)}{k_2} + \frac{t_1}{k_5} + \frac{t_3}{\omega+\mu}.
\end{aligned}
$$

The equation $H(\lambda^*) = 0$ in (22) admits the trivial solution $\lambda^* = 0$, which corresponds to the disease-free equilibrium (E_0) defined in (14). Any additional non-negative real roots of $P(\lambda^*) = 0$, when they exist, correspond to endemic equilibrium points of the system. From the coefficient expressions in (24), we observe that $Q_0 > 0$ when $\mathcal{R}_0 < 1$, and Q_3 remains positive for all parameter values.

To investigate the possibility of multiple endemic equilibria, we apply Descartes' rule of signs to the cubic polynomial $P(\lambda^*)$ given in (23). This classical method enables us to systematically determine the number of positive real roots by examining sign changes in the sequence of polynomial coefficients under various parameter regimes. In particular, the signs of Q_1, Q_2 and the value of $\mathcal{R}_0$ play a critical role in determining the root structure of $P(\lambda^*)$. Table 2 summarizes the different cases, classifying the number of possible positive real roots based on these key parameters.

Theorem 3.5 follows directly from the classification of root structures summarized in Table 2.

Theorem 3.5.
Consider the model (11). Then,

1. *the model admits a unique endemic equilibrium if cases 1, 2, or 4 occur with $\mathcal{R}_0 > 1$.*
2. *the model may admit multiple endemic equilibria if case 3 occurs with $\mathcal{R}_0 > 1$.*
3. *the model may admit multiple endemic equilibria if cases 2, 3, or 4 occur with $\mathcal{R}_0 < 1$.*
4. *the model admits no endemic equilibrium if case 1 occurs with $\mathcal{R}_0 < 1$.*

Remark 3.6. Item (3) of Theorem 3.5 establishes the co-existence of disease-free equilibrium and one or more endemic equilibria when $\mathcal{R}_0 < 1$. This implies that the system (11) may exhibit a backward bifurcation phenomenon, where the disease can persist in the population even though the basic reproduction number is below the classical threshold of unity. In such cases, reducing $\mathcal{R}_0$ below one is not sufficient to guarantee disease elimination, and additional control measures may be required to steer the system towards the disease-free-equilibrium.

The phenomenon of a backward bifurcation in the model (11) is formally established in Theorem 3.7.

Theorem 3.7. *The model (11) exhibits a backward bifurcation at $\mathcal{R}_0 = 1$.*

The proof of Theorem 3.7, which relies on the center manifold theory and Theorem 4.1 of [25], is provided in Appendix C. Furthermore, the existence of a backward bifurcation for $\mathcal{R}_0 < 1$ is demonstrated numerically in Fig. 2.

When there is no reinfection (i.e. $\omega = 0$) and the vaccine is perfect (i.e. $\rho = 1$), the model (11) does not exhibit a backward bifurcation. Under these conditions, the disease-free equilibrium is globally asymptotically stable for $\mathcal{R}_0 < 1$, as stated in Theorem 3.8, with the proof provided in Appendix D based on the LaSalle Invariance Principle [26].

Theorem 3.8. *Under the assumption $\omega = 0$ and $\rho = 1$, the disease-free equilibrium, E_0 of the model (11) is globally asymptotically stable whenever $\mathcal{R}_0 < 1$.*

Numerical simulation illustrating the global asymptotic stability of the disease-free equilibrium for $\mathcal{R}_0 < 1$ under the conditions $\omega = 0$ and $\rho = 1$ is presented in Fig. 2.

When reinfection is absent ($\omega = 0$) and vaccines confer perfect immunity ($\rho = 1$), the coefficients in the polynomial Eq. (23) simplify

Table 2
Number of possible positive roots for (23).

Cases	$\mathcal{Q}_3$	$\mathcal{Q}_2$	$\mathcal{Q}_1$	$\mathcal{Q}_0$	$\mathcal{R}_0$	No of sign changes	No of possible equilibrium (roots)
1	+	+	+	+	<1	0	0
	+	+	+	−	>1	1	1
2	+	+	−	+	<1	2	0, 2
	+	+	−	−	>1	1	1
3	+	−	+	+	<1	2	0, 2
	+	−	+	−	>1	3	1, 3
4	+	−	−	+	<1	2	0, 2
	+	−	−	−	>1	1	1

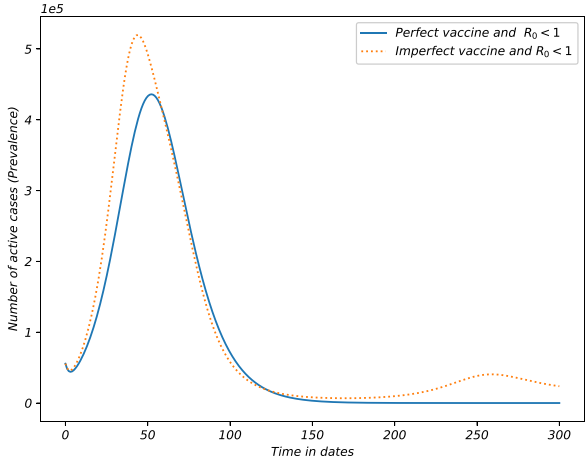

Fig. 2. Stability analysis of the disease-free equilibrium (DFE) comparing perfect vaccination ($\rho = 1$, $\omega = 0$) with imperfect vaccination. Although both scenarios satisfy $\mathcal{R}_0$, the system under perfect vaccination (blue curve) shows global DFE stability, while imperfect vaccination (orange curve) leads to bistability — coexistence of DFE and endemic equilibria — indicating backward bifurcation. This illustrates how vaccine efficacy (ρ) and waning immunity (ω) critically affect eradication thresholds. (For interpretation of the references to color in this figure legend, the reader is referred to the web version of this article.)

such that $\mathcal{Q}_3 = 0$, $\mathcal{Q}_2 > 0$ and $\mathcal{Q}_1 > 0$. According to Table 2, this configuration ensures a unique positive root of (23). Consequently, the system (11) admits a unique endemic equilibrium E^*;

$$E^* = (S^*, V^*, A^*, I^*, 0, 0, Q^*, R^*) \tag{25}$$

for $\mathcal{R}_0 > 1$. This implies that under these conditions, the model does not exhibit a backward bifurcation, even when the basic reproduction number exceeds unity. In this case, the total population size N, the force of infection λ and the basic reproduction $\mathcal{R}_0$ simplify to

$$N = S + V + A + I + Q + R, \tag{26}$$

$$\lambda = \beta \frac{I + \nu A}{N}, \tag{27}$$

$$\mathcal{R}_0 = \frac{\nu B_1}{k_1} + \frac{B_2}{k_2}. \tag{28}$$

Consequently, the following remark follows from the preceding discussion and Theorem 4.1, item (iv), of [25].

Remark 3.9. For the model (11), a unique endemic equilibrium exists and is locally asymptotically stable, provided that $\mathcal{R}_0 > 1$ and $\mathcal{R}_0$ is sufficiently close to unity.

The next theorem establishes that perfect vaccination (i.e, $\rho = 1$) and the absence of reinfection (i.e, $\omega = 0$) can suppress disease transmission, even when $\mathcal{R}_0 > 1$.

Theorem 3.10. *For $\rho = 1$ and $\omega = 0$, let $I^* = I^*(\sigma)$ denote the infectious component of the endemic equilibrium corresponding to the vaccination rate parameter σ. Then we have*

$$I^*(\sigma) < I^*(0),$$

that is, increasing vaccination rate reduces the infectious population at equilibrium.

Proof. When $\rho = 1$, the endemic equilibrium point is given by

$$E^* = (S^*, V^*, A^*, I^*, 0, 0, Q^*, R^*),$$

and from Eq. (18), the conservation law yields

$$\Lambda - \mu N^* - \delta(I^* + Q^*) = 0,$$

where $N^* = S^* + V^* + A^* + I^* + Q^* + R^*$. Rearranging, we get

$$(\mu + \delta)I^* = \Lambda - \mu(S^* + V^* + A^* + R^*) - (\mu + \delta)Q^*.$$

Thus, the infectious component at equilibrium as a function of σ is

$$I^* = I^*(\sigma) = \frac{\Lambda - \mu(S^* + V^* + A^* + R^*) - (\mu + \delta)Q^*}{\mu + \delta}.$$

Since the vaccination rate σ affects V^* but not other components, we have

$$\begin{aligned} I^*(\sigma) &= \frac{\Lambda - \mu(S^* + V^* + A^* + R^*) - (\mu + \delta)Q^*}{\mu + \delta} \\ &\leq \frac{\Lambda - \mu(S^* + A^* + R^*) - (\mu + \delta)Q^*}{\mu + \delta} = I^*(0). \end{aligned}$$

This completes the proof. □

4. Model fitting

This study develops an epidemiological model to assess COVID-19 vaccine effectiveness, calibrated and validated using case data from South Africa. Although the analysis focuses on South Africa, the vaccines deployed in the county, such as Pfizer-BioNTech, Johnson & Johnson, Oxford-AstraZeneca, among others, were also central to global vaccination efforts, spanning high-income countries (e.g., United States, United Kingdom) to middle-income nations (e.g., Brazil, India).

Despite delayed rollouts in Africa and other low-income regions, many of which relied heavily on WHO's COVAX initiative for vaccine supply, the same vaccines were deployed as in wealthier countries. However, real-world effectiveness varied substantially across populations due to factors like variant prevalence, healthcare infrastructure, and demographic differences [27–30]. Therefore, while our findings should not be generalized as universal vaccine performance metrics, the model remains applicable to countries with similar vaccination strategies, such as Botswana and Namibia.

COVID-19 case data for South African were obtained from the Johns Hopkins University COVID-19 repository [17]. The analysis follows a three phase approach:

(1) Data Presentation, providing an overview of calibration datasets including case counts and vaccination timelines.
(2) Parameter Estimation, with initial parametrization based on WHO and CDC guidelines, as well as published literature.
(3) Model Fitting, where parameter estimates are refined through least-squares optimization implemented via the Python *lmfit* library.

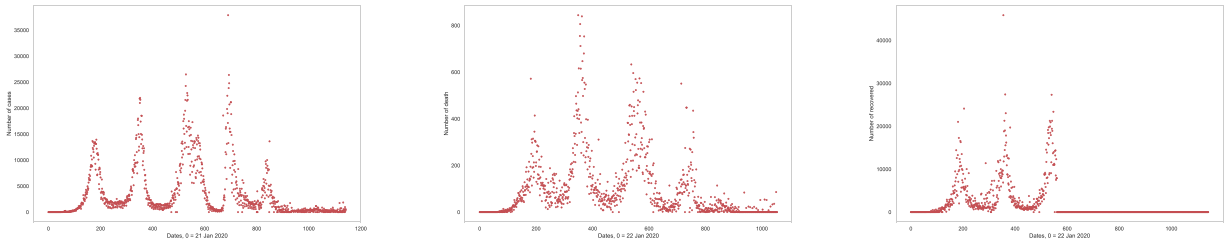

(a) South African Daily infection data (b) South African Daily death data (c) South African Daily recovery data

Fig. 3. South African daily COVID-19 data from [17].

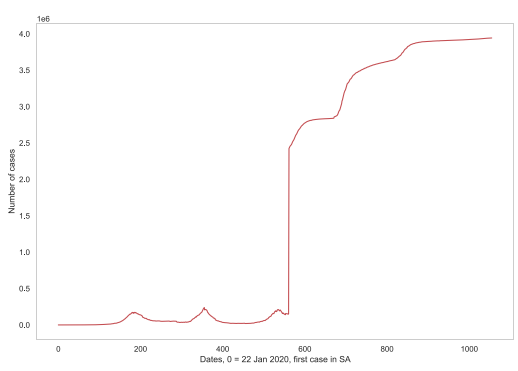

(a) Active South African COVID19 cases from 22 January 2020 to 18 November 2022.

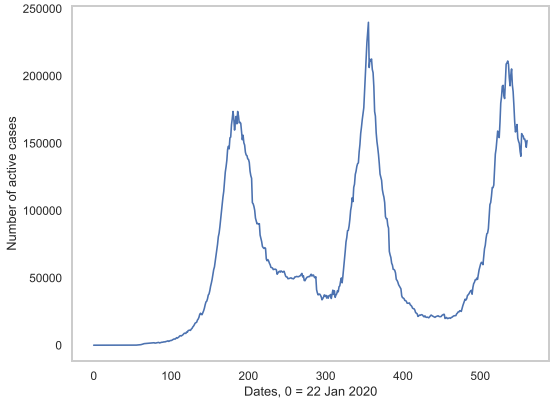

(b) Active South African cases from 22 Jan 2020 to 5 August 2021.

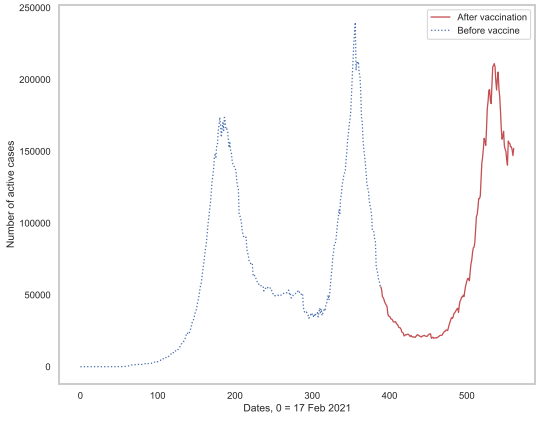

(c) The blue portion represents the data before vaccines introduced in South Africa

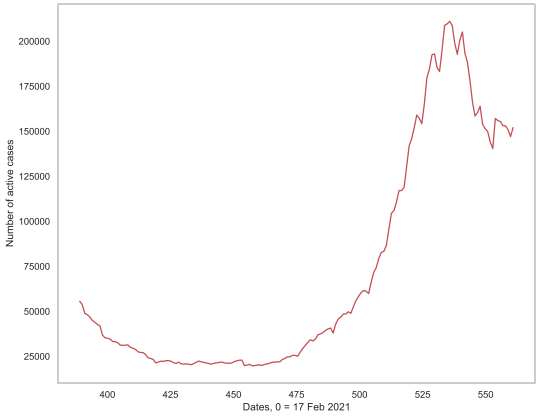

(d) Active South African cases between 17 Feb 2021 and 5 August 2021.

Fig. 4. South African COVID-19 data.

4.1. About the data

Global COVID-19 data, publicly available from Johns Hopkins University [17], were downloaded and processed using Python. Fig. 3 presents South Africa's daily COVID-19 statistics, including reported daily infections, recoveries, and deaths. During data processing, we identified a discontinuity in the daily recovery records beginning on day 561 (relative to January 22, 2020, the date of South Africa's first reported case), which corresponds to August 5, 2021. This anomaly results in an artificial spike in active cases on day 561, as illustrated in Fig. 4(a). To ensure consistency in subsequent analysis, the dataset was truncated at day 561 (see Fig. 4(b)).

The South African vaccine data were also obtained from the same Johns Hopkins University database [17]. The first COVID-19 vaccines were administered in South Africa on February 17, 2021. Since our goal is to analyze the impact of vaccinations, we focus on the data recorded between February 17, 2021 and August 5, 2021 as this period contains a complete record of vaccination data and active cases data. This subset of the daily vaccination data is shown in Fig. 5. Fig. 4(c) highlights the periods before and after the introduction of vaccines, while Fig. 4(d) presents the daily active cases for the first 172 days since the start of vaccination campaign (February 17–August 5, 2021,).

4.2. Initial parameter estimation

To set our initial parameter estimations, we used data and literature from various credible sources.

According to the latest World Bank estimate [31], the South African population is approximately 60.2 million, with an annual growth rate

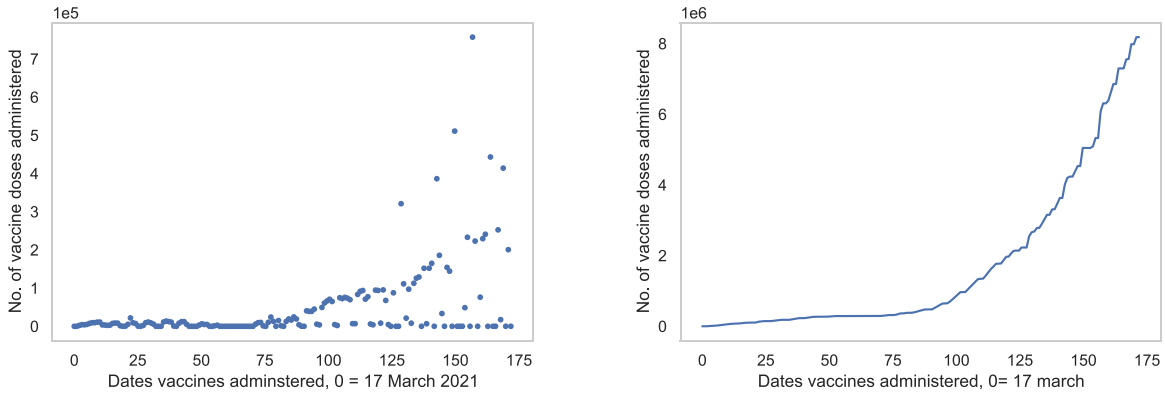

(a) Daily vaccination time series

(b) Total vaccination time series

Fig. 5. South African vaccination data for the first 172 days.

of 1.2% and annual death rate of 9.468/1000. This yields a daily recruitment rate

$\Lambda \approx 3583.3$

and daily non-COVID related death rate of

$\mu \approx 2.6433 \times 10^{-5}$.

The daily vaccination rate, σ, is estimated by the daily average of vaccine doses administered per day between February 17 and August 5, 2021 (Fig. 5). During this 172 day period, South Africa administered 8182380 doses of vaccines doses. Thus, the estimated vaccination rate is

$\sigma \approx 7.9 \times 10^{-4}$.

It is well known that non of the COVID-19 vaccines provided full protection against infection, but they significantly reduced symptom severity and improved recovery outcomes [32,33]. Early reports considerable variation in vaccine effectiveness. According to WebMed [34], the efficacy of the WHO approved vaccines ranged from approximately 50% to 95%; see also [35–37]. We adopted the midpoint of this range, $\rho = 0.75$ as our initial estimate for vaccine effectiveness. To define a plausible fitting range, we considered the possibility that real-world effectiveness may be lower than reported due to uncontrolled circumstances, such as variant prevalence, delayed dosing, or storage issues. Based on this, we selected the interval $(0.3, 1)$ as our fitting range for ρ.

To estimate the proportion of symptomatic and asymptomatic infection in the population, we use a result from the case study conducted on a specific workplace setting [38]. According to this study, 36.6% of the infected individuals remain asymptomatic through out their infection, while up to 45% are asymptomatic in the first few days. Based on these findings, we assume that 45% of all infections are asymptomatic. Among these, 81.3% remain asymptomatic throughout their infection, while the remaining 18.7% develop mild symptoms that prompt them to seek testing within one week, subsequently transitioning to compartment Q. Accordingly, we set the initial estimates as $\eta = 0.45$ and $\theta = 0.187/7 = 0.0267$, with fitting ranges of $(0.3, 0.6)$ for η and $(0.01, 0.03)$ for θ.

The authors were unable to identify a publicly available study that specifically estimates the asymptomatic-to-symptomatic infection proportion among vaccinated individuals. However, based on reports from the World Health Organization and other sources, vaccines are known to reduce the severity of symptoms and the risk of fatal outcomes. Consequently, we assume that the proportion of asymptomatic infections among vaccinated individuals, ϕ, is greater than that of the general population, i.e., $\phi > \eta$. In particular, we set $\phi \approx 0.5$ as an initial estimate and define the fitting range $(\eta, 1)$.

According to [39] and the Department of health of South Africa, individuals who test positive for COVID-19 are required to isolate for a minimum of 10 days. Based on this guideline, we assume that individuals in compartment Q remain in isolation for approximately 10–15 days. Considering that the overall COVID-19 has a recovery rate is estimated at 97.4% [1], we define the fitting range for the recovery rate parameter γ_3 as $(0.0694, 0.0974)$ and set an initial estimation of $\gamma_3 = 0.09$.

According to [40], the recovery period for asymptomatic patients ranges from 1–2 weeks, with the median duration of 9 days. Based on this, we assume a fitting range of $(0.0544, 0.1167)$ for the recovery rate of asymptomatic individuals, γ_1 and set the initial estimate to $\gamma_1 = 1/9 \times 0.813 = 0.0903$.

Furthermore, according to [1], the overall recovery rate in South Africa is about 97.4%, and according to [41], the median time to death for non-survivors is 18.5 days. Based on these reports, we define the fitting range for the death rate δ as $(0.0012, 0.0016)$ as our fitting range and $\delta = 0.0015$, as an initial estimate.

Given that vaccination reduces the risk of death, we assume that the death rate among vaccinated individuals, δ_1, is lower than that of the general population, i.e., $\delta_1 < \delta$. Therefore, we set the fitting range for δ_1 as $(0, \delta)$ and take $\delta_1 = 0.0011$ as an initial estimate.

Next, we estimate the parameters $\epsilon, \epsilon_1, \gamma_2, \gamma_4, \gamma_5,$ and θ_1.

Hypothetically, every individual in compartment I is expected to experience some level of discomfort or pain. As a result, most of them would either choose to self-isolate or use government facilities to protect their loved ones or require hospitalization due to the severity of symptoms. We assume that only 25% of these individuals recover with out entering isolation, while the majority transition to compartment Q. Assuming that such transitions occur with in a week, we define the fitting range for ϵ as $(0.1051, 0.1472)$ and set the initial estimate as $\epsilon = 0.1252$.

According to [42,43], the recovery period for symptomatic individuals ranges from 8 to 37 days, with a median of approximately 20 days. Based on this, we define the fitting range for the recovery rate parameter γ_2 as $(0.0066, 0.0313)$ and use $\gamma_2 = 0.0125$ as an initial estimate.

To estimate the remaining parameters, such as $\theta_1, \epsilon_1, \gamma_4$ and γ_5, we assume individuals in compartment I_1 transition to compartments Q and R in equal proportion. However, due to vaccination, they are expected to recover quickly than their unvaccinated counterparts. Following a similar rationale to that used for compartment I, and assuming that individuals self-isolate within 2 to 7 while those who do not isolate recover with in 8 to 38 days, we define the fitting ranges as $\epsilon_1 \in (0.1057, 0.37)$ and $\gamma_5 \in (0.0066, 0.0313)$. We set the initial estimates as $\epsilon_1 = 0.125$, $\gamma_5 = 0.0275$.

Finally, by employing an approach analogous to the one used for estimating θ and γ_1, we determine the fitting ranges $\theta_1 \in (0.01, 0.1)$ and

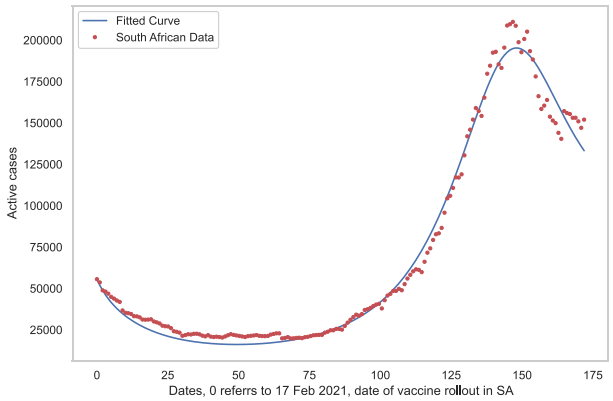

Fig. 6. The model fitted to the South African Covid-19 Data from 17 Feb to 5 Aug 2021.

$\gamma_4 \in (0.0544, 0.1167)$, with initial estimates $\theta_1 = 0.0267$ and $\gamma_4 = 0.095$. A summary of all parameter estimates and their corresponding fitting ranges is provided in Table 3.

4.3. Fitting the model to the South African data collected on days 17 Feb 2021–5Aug 2021

Although our parameter estimation is primarily data-driven and supported by relevant literature, further refinement within the specified range is necessary through model fitting. The model is calibrated using the data shown in Fig. 4(d), which corresponds the relevant time period, i.e., February 17–August 5, 2021. The fitting procedure is carried out using the open-source Python library *lmfit*. Table 3 summarizes both the initial parameter estimates, as outlined in Section 4.2, and their optimized values obtained through the fitting process. The results of the fitting are shown in Fig. 6, which illustrates that the model effectively captures the observed transmission dynamics.

Since the primary goal of this analysis is to assess vaccine effectiveness through a mathematical model approach, particular emphasis is placed on parameters related to vaccination, namely, ρ, δ_1, γ_4, and γ_5. The parameters γ_4 and γ_5 represent the rate at which vaccinated individuals transition to the recovered compartment (R), while δ_1 denotes the COVID-19-induced mortality rate among vaccinated individuals. Lastly, the parameter ρ quantifies the effectiveness of vaccines in preventing infection.

According to WHO, CDC, and other sources [27–29], vaccine effectiveness varies based on several factors, including the number of doses administered, the type of vaccine, the time elapsed since vaccination, the characteristics of the vaccinated population, and, most critically, the COVID-19 variant. Reports from the WHO and the National Institute for Communicable Diseases of South Africa indicate that the beta variant was dominant from February to May 2021, while the Delta variant was dominant from June to August 2021. For further details on variant prevalence in South Africa, see [44], and for insights into incorporating COVID-19 variants into epidemiological models and their impact on vaccine effectiveness, refer to [30] and the references in there. These studies report vaccine efficacy ranging from as high as 95% to as low as 50%, depending on the variant and other influencing factors. Importantly, such reported efficacy generally reflects the vaccines combined ability to prevent symptomatic infection and to reduce the risk of hospitalization and death.

However, a recent report from the National Center for Immunization and Respiratory Diseases (NCIRD), published on February 1, 2024 [45] highlights improvements in COVID-19 vaccine performance. Based on data collected from mid-September 2023 to January 2024, the report states that individuals vaccinated with recent vaccine formulations were about 54% less likely to get infected with the virus. Given this, we anticipate that our model fitting will yield an estimated effectiveness rate for preventing infection that is below 54%.

In our model fitting, particular attention was given to the parameter ρ, which represents the effectiveness of vaccines in preventing infection. Although, in theory, ρ can range from 0 to 1, it is unreasonable to assume that vaccines with 0% effectiveness would have received regulatory approval or widespread distribution. Taken into account the urgency and uncertainty present during the initial stages of vaccine rollout, we allowed ρ to vary between 0.3 and 1, as specified in Section 4.2. This range accommodates potential variations in vaccine performance, even though existing literature reports effectiveness rates typically ranging from 50% to 95%.

The fitted result suggests that $\rho \approx 0.3000$, which is lower than the reported effectiveness of currently produced vaccines [45], as anticipated. This outcome aligns with the understanding that ρ in our model specifically captures vaccine effectiveness in preventing infection, rather than the broader efficacy metrics reported in clinical studies. Additionally, the fitted parameters suggest $\gamma_2 = 0.0066$ and $\gamma_5 = 0.0232$, indicating that individuals in compartment I_1 (vaccinated and infected) recover more rapidly than those in compartment I (unvaccinated and infected). This supports the reports from WHO and CDC that vaccination reduces disease severity. Furthermore, the results yield $\delta = 0.0012$ and $\delta_1 = 2.02 \times 10^{-14} \approx 0$, highlighting the significant protective effect of vaccination in reducing COVID-19 related mortality. These findings underscore the vital role of vaccines in saving lives during the pandemic.

Thus, these results support the conclusion that vaccines have played a significant role in reducing both disease severity and mortality. This is evident from the relationship $\gamma_2 \ll \gamma_5$, indicating faster recovery among vaccinated individuals, from $\delta_1 \lll \delta$, reflecting a dramatic reduction in COVID-19 induced mortality due to vaccination. However, since $\rho < 0.5$, the effectiveness of vaccines in preventing infection appears to be lower than initially anticipated. But, as mentioned earlier, this could also be due to the new delta variant that appeared immediately after the introduction of vaccines [30]. For further discussion and concluding remarks, the reader is referred to Section 6.

5. Local sensitivity analysis

In this section, we analyze the sensitivity of the basic reproduction number $\mathcal{R}_0$ to slight changes in the parameters involved in Eq. (16). This is achieved by computing the partial derivative of $\mathcal{R}_0$ with respect to a parameter of interest, say p. The resulting quantity

$$\frac{\partial \mathcal{R}_0}{\partial p}$$

is referred to as the local sensitivity index of $\mathcal{R}_0$ with respect p, and is denoted by $\gamma_p^{\mathcal{R}_0}$ (see [46]), i.e.,

$$\gamma_p^{\mathcal{R}_0} = \frac{\partial \mathcal{R}_0}{\partial p}.$$

for a better reflection of the correlation between $\mathcal{R}_0$ and parameter p, we consider the normalized sensitivity index, denoted by $\epsilon_p^{\mathcal{R}_0}$, which is defined as

$$\epsilon_p^{\mathcal{R}_0} := \frac{\partial \mathcal{R}_0}{\partial p}\frac{p}{\mathcal{R}_0}.$$

This normalized index expresses the relative changes in $\mathcal{R}_0$ resulting from relative changes in p. In particular, $\epsilon_p^{\mathcal{R}_0}$ quantifies the percentage change in $\mathcal{R}_0$ when p is changed by a certain percent, say $y\%$ (see [46, 47]). That means that

$$\Delta \mathcal{R}_0\% = \epsilon_p^{\mathcal{R}_0} y\%,$$

or equivalently,

$$\epsilon_p^{\mathcal{R}_0} = \frac{\Delta \mathcal{R}_0\%}{\Delta p\%}.$$

The local sensitivity index of $\mathcal{R}_0$ is summarized in Table 3, which shows the relationship between each of the parameter and $\mathcal{R}_0$. A visual representation of these indices is provided in Fig. 8. A negative sensitivity index, $\epsilon_p^{\mathcal{R}_0}$, indicates that $\mathcal{R}_0$ and the parameter p are inversely related, while a positive sensitivity index implies a direct relationship. Moreover, the absolute value of $\epsilon_p^{\mathcal{R}_0}$ reflects the relative influence of parameter p on the basic reproduction number $\mathcal{R}_0$: larger values suggest greater sensitivity.

Since our goal is to assess the contribution of vaccination, we focused particularly parameters associated with vaccination, such as ρ, ϕ, θ_1, ϵ_1, γ_4 and γ_5. Using the basic reproduction number $\mathcal{R}_0$ as a response function, several key conclusions can be drawn from the sensitivity indices summarized in Table 3 and visualized Fig. 8.

Fig. 8 highlights the significance of parameters ρ, ϕ, θ_1, γ_4, ϵ_1, β, ν_1 and κ. Notably, the relatively large sensitivity index $\epsilon_\phi^{\mathcal{R}_0}$ compared to $\epsilon_\eta^{\mathcal{R}_0}$ suggests that vaccinated individuals with asymptomatic infections contributed substantially to ongoing transmission. In addition, the sensitivity indices $\epsilon_{\theta_1}^{\mathcal{R}_0}$ and $\epsilon_{\epsilon_1}^{\mathcal{R}_0}$ underscore the importance of identifying and isolating infected individuals, even those who are vaccinated, in mitigating disease spread.

The parameter, ρ which represents vaccine effectiveness of vaccines in preventing infection, is inversely related to $\mathcal{R}_0$. Thus, improving ρ would significantly reduce disease transmission. The relatively small value of ρ, combined with the large $|\epsilon_\rho^{\mathcal{R}_0}|$, underscores the importance of continued research aimed at developing more effective vaccines or enhancing the efficacy of existing ones.

To further understand the role of vaccination, we compare some of the parameters with their unvaccinated counterparts. From Table 3, we observe that

$$|\epsilon_\theta^{\mathcal{R}_0}| < |\epsilon_{\theta_1}^{\mathcal{R}_0}| \quad \text{and} \quad |\epsilon_\epsilon^{\mathcal{R}_0}| < |\epsilon_{\epsilon_1}^{\mathcal{R}_0}|.$$

This suggests that identifying and isolating vaccinated individuals who become infected may have an even greater impact on reducing transmission than similar efforts among unvaccinated individuals. These findings highlight the need for continued monitoring of vaccinated individuals, along with public awareness campaigns that emphasize the imperfect nature of vaccine protection and encourage regular testing to determine infection status.

We now turn to interpreting the daily infection data and prevalence data presented in Fig. 7. An examination of the daily infection data reveals that the peaks of successive waves continued to rise even after the introduction of vaccines, up to the fourth wave (see Fig. 7(b)). However, the trend in daily prevalence data shows the opposite; a steady decline over the same period. This apparent discrepancy suggests that although the number of new daily infections increased, the overall recovery rate also improved significantly, leading to lower net prevalence. Our model supports this interpretation, indicating that recovery rates increased and death rates declined following the rollout of vaccines. For complete records of prevalence and mortality data, we refer the reader to the worldometer database [1].

An unexpected, though not significant, observation is the positive relation between the vaccination rate parameter σ and the basic reproduction number $\mathcal{R}_0$. One possible explanation for the positive sensitivity index $\epsilon_\sigma^{\mathcal{R}_0}$ is that vaccinated individuals, due to incomplete protection against infection, still contribute to transmission, particularly through asymptomatic infections. Despite this, vaccination remains critical; our model indicates that the improvement in recovery rates following vaccination led to decline in prevalence and ultimately helped curb the spread of the disease. Thus, the implementation of the vaccine program was essential for reducing mortality and saving lives. Furthermore, the sensitivity indices $\epsilon_{\nu_1}^{\mathcal{R}_0}$ and $\epsilon_\kappa^{\mathcal{R}_0}$ highlight another important aspect; vaccinated individuals, feeling relatively safe, may have increased their contact with the public. If infected, such behavior could enhance transmission, contributing to the observed positivity of $\epsilon_\sigma^{\mathcal{R}_0}$. This underlines the importance of continued public health messaging, even in highly vaccinated populations, to mitigate behavioral risks.

Based on the findings of this study, we conclude that greater public and stakeholder awareness of the actual level of protection provided by COVID-19 vaccines at the time could have led to a different trajectory of disease spread. If individuals had understood that vaccine effectiveness might be lower than 50%, rather than assuming it was above 50%, they may have adopted additional protective measures to safeguard themselves and those around them. For further concluding remarks, we refer to Section 6.

6. Conclusion

In this study, we developed and analyzed a mathematical model that captures the imperfect efficacy of COVID-19 vaccines, incorporating key features such as waning immunity and breakthrough infections to evaluate their impact on pandemic trajectory in South Africa. The model integrates multiple dimensions of disease dynamics, including viral transmission, vaccine mediated protection against severe outcomes, public health containment measures, and alignment with WHO and CDC guidelines. Although the model was calibrated using South African case data, a decision motivated by the authors' regional familiarity and data availability, its structure sufficiently flexible to be adapted to other settings that deployed similar vaccines and implemented comparable distribution strategies.

The model was analyzed both theoretically and numerically. The theoretical analysis demonstrated that when vaccines are imperfect, the model may exhibit a backward bifurcation even when the basic reproduction number $\mathcal{R}_0 < 1$ (see Theorems 3.5 and 3.7). However, in the absence of a backward bifurcation, the disease-free equilibrium is shown to be globally asymptotically stable whenever $\mathcal{R}_0 < 1$ (see Theorem 3.8). Remark 3.9 establishes the existence of at least one locally asymptotically stable endemic equilibrium when $\mathcal{R}_0 > 1$ and close to unity. Furthermore, the positive impact of perfect vaccination in reducing disease prevalence is demonstrated in Theorem 3.10.

For numerical analysis, we fitted the South African COVID-19 data to model (11). The parameter estimation results indicate that vaccination significantly improved recovery outcomes, with vaccinated individuals experiencing faster recovery ($\gamma_5 > \gamma_2$) and lower mortality ($\delta_1 < \delta$) compared to their unvaccinated counterparts (see Table 3, rows 7, 10, 18, and 19). These results provide quantitative confirmation that vaccination reduces both disease severity and the risk of death.

The local sensitivity indices of $\mathcal{R}_0$ with respect to the model parameters were computed to identify those with greatest influence. The result indicate that the parameters ϕ, β, ν_1, κ, ρ, γ_4, θ_1 and ϵ_1 are the most significant. Among these, ϕ, β, ν_1 and κ are positively correlated with $\mathcal{R}_0$, while ρ, γ_4, θ_1 and ϵ_1 are negatively correlated. This yields the following proportional relationships:

$$\mathcal{R}_0 \propto \beta,\ \nu_1,\ \kappa \quad \text{and} \quad \mathcal{R}_0 \propto \frac{1}{\rho},\ \frac{1}{\epsilon_1},\ \frac{1}{\gamma_4}.$$

A graphical representation of these relationships is provided in Fig. 10.

Therefore, an effective intervention strategy should aim to reduce the value of parameters β, ν_1, and κ, while enhancing the protective parameters ρ, γ_4, θ_1 and ϵ_1. The following measures could contribute to achieving these objectives:

Support vaccine research and development: investing in scientific research to produce more effective vaccines can help increase the value of ρ, thereby enhancing protection against infection (see Fig. 9).

Promote adherence to public health guidelines: Encouraging the public to follow WHO recommended non-pharmaceutical interventions, such as avoiding unnecessary social contact even after vaccination can contribute to reducing the transmission rate β.

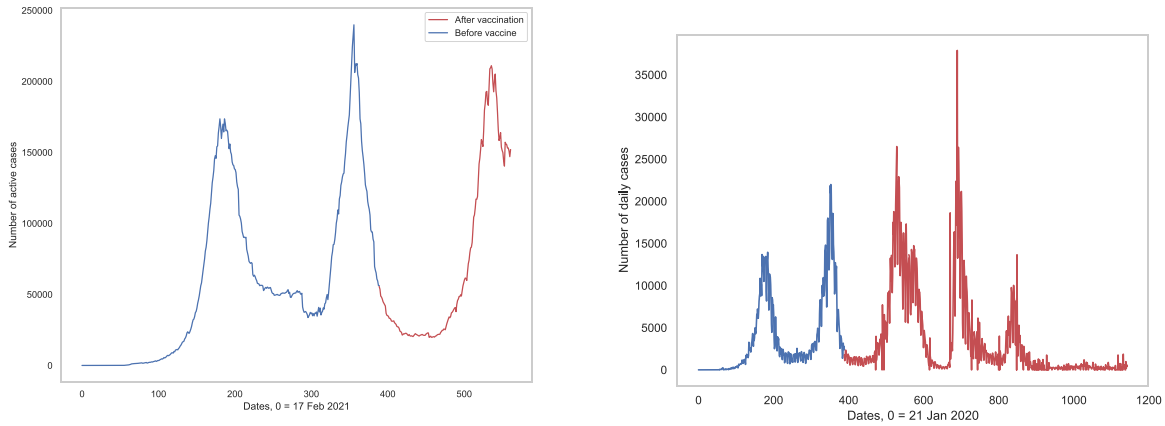

(a) South African Active cases until 5 August 2021

(b) South African daily infection cases until recently

Fig. 7. South African Active and daily infection data.

Table 3
Initial estimate of involved parameters, their possible range according to literature, their fitted values and sensitivity index of $\mathcal{R}_0$ with respect to the involved parameters.

No.	Param	Initial estimate	Fitting range	Fitted value	$\gamma^{\mathcal{R}_0}_{param}$	$\epsilon^{\mathcal{R}_0}_{param}$	Source
	Λ	3538.3	N/A	N/A	0	0	calculated
	σ	7.9×10^{-4}	N/A	N/A	185.9	0.0242	calculated
	μ	2.6433×10^{-5}	N/A	N/A	−5603.6	−0.0244	calculated
	θ	0.0267	(0.01,0.03)	0.03	−0.0847	−0.0004	fitted
	θ_1	0.0267	$(0.01, \theta)$	0.01	−23.2	−0.0382	fitted
	γ_1	0.0904	(0.0544,0.1167)	0.1167	−0.0847	−0.0016	fitted
	γ_2	0.0175	(0.0066,0.0313)	0.0066	−0.3303	−0.0004	fitted
	γ_3	0.09	(0.0694,0.0974)	0.0974	0	0	fitted
	γ_4	0.095	(0.0544,0.1167)	0.1141	−23.20	−0.4354	fitted
	γ_5	0.0275	(0.0066,0.0313)	0.0233	−0.0847	−0.0934	fitted
	ω	1/120	N/A	N/A	0	0	[48]
	φ	0.0022	$(0.0011, \omega)$	0.0011	0	0	fitted
	ϕ	0.5	$(\eta, 1)$	0.468	0.2337	0.018	fitted
	ρ	0.75	(0.3,1)	0.300	−8.612	−0.4251	fitted
	η	0.45	(0.3,0.6)	0.30	−0.0121	−0.0006	fitted
	ϵ	0.1252	(0.1057,0.1472)	0.1057	−0.3303	−0.0057	fitted
	ϵ_1	0.1252	(0.1057,0.1472)	0.1057	−24.413	−0.4246	fitted
	δ	0.0015	(0.0012,0.0016)	0.0012	−0.3303	−0.00	fitted
	δ_1	0.0011	$(0, \delta)$	0.0	−24.414	−0.00	fitted
	β	0.9	(0,3)	0.1878	32.36	1.0	fitted
	ν	3.5	(0,6)	1.0	0.0124	0.0021	fitted
	ν_1	3.5	(0,6)	6.0	0.4799	0.4737	fitted
	κ	1.25	(1,6)	6.0	0.5248	0.5181	fitted

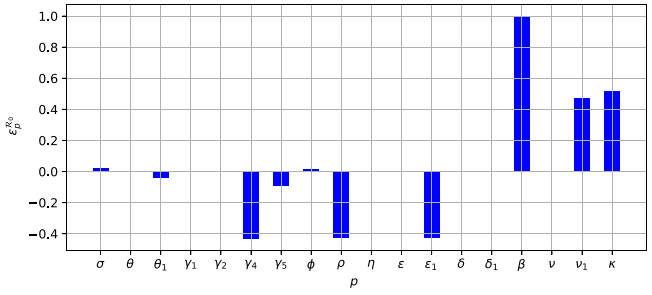

Fig. 8. Graphical representation of the sensitivity index of $\mathcal{R}_0$.

Raise awareness of vaccine limitations: Educating the public about the actual efficacy levels of COVID-19 vaccines can reduce overconfidence among vaccinated individuals. This can lead to a reduction in ν_1 and κ, as more cautions behavior among vaccinated individuals lowers the risk of virus transmission.

Expand testing and contact tracing: Increasing the frequency of testing, especially among vaccinated individuals, and implementing effective contact tracing can help identify and isolate infected persons. This would enhance the detection and isolation rates θ_1 and ϵ_1, ultimately contributing to the reduction of $\mathcal{R}_0$ (see Fig. 10).

In general, based on both numerical and theoretical analysis of our model, we draw the following conclusions:

(1) The result $\delta > \delta_1$ indicates that vaccines improved recovery rate. This finding aligns with official reports from the WHO and CDC, such as [32,49].
(2) The estimate $\rho \approx 0.3$ suggests that vaccines did not provide complete protection from COVID-19 infection, highlighting the need for continued research to enhance vaccine efficacy. This observation is also consistent with findings from the NCIRD report [45].
(3) The result $\gamma_5 > \gamma_2$ shows that vaccinated individuals recover more quickly and have a reduced risk of mortality. This outcome is also supported by WHO and CDC data [32,49].

Based on the results of this work, we recommend that public health policy makers and other stakeholders consider the following points in their strategic planning:

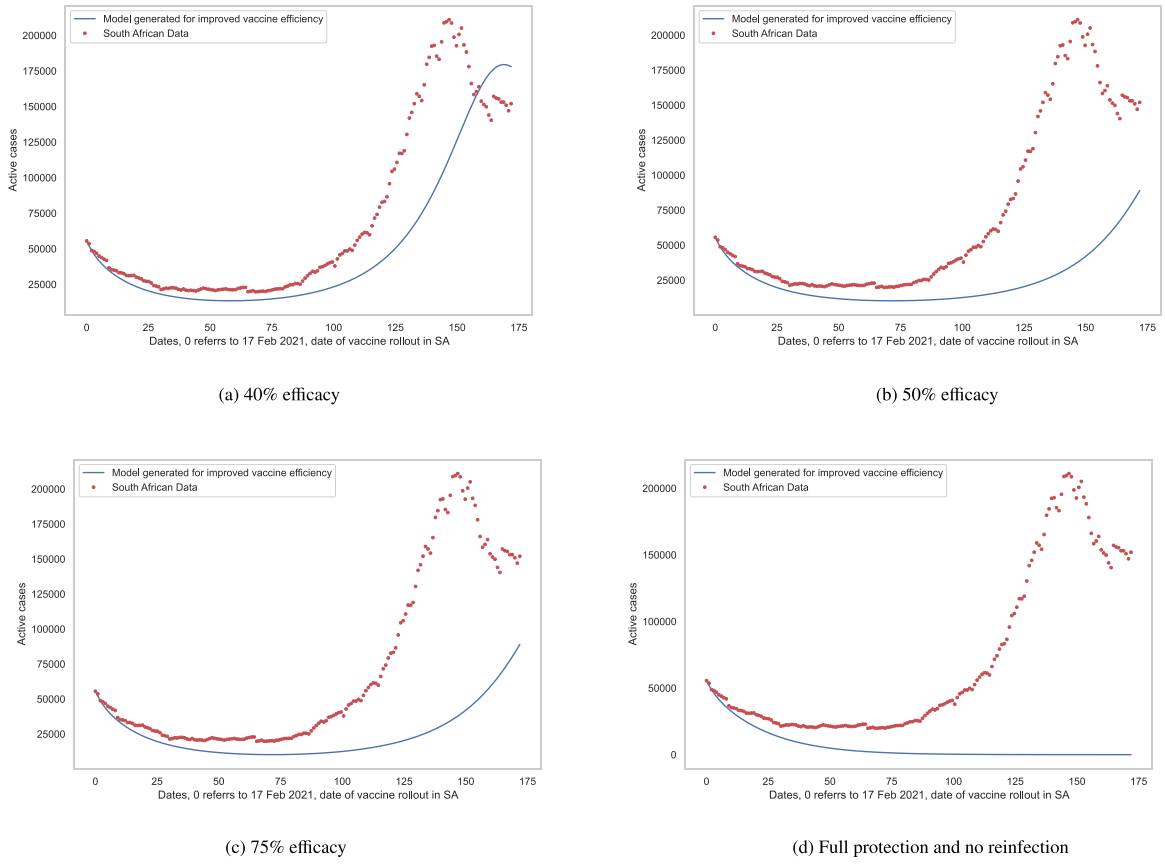

(a) 40% efficacy

(b) 50% efficacy

(c) 75% efficacy

(d) Full protection and no reinfection

Fig. 9. Different efficacy levels were considered to demonstrate the role that vaccines could play in flattening the curve and delaying the peak.

(1) Encourage the public to reduce mobility and social interactions when feasible to limit contact with potential infectious individuals, especially in the event of future outbreaks. This aligns with the fact that $\mathcal{R}_0 \propto \beta$, $\mathcal{R}_0 \propto \nu$, $\mathcal{R}_0 \propto \nu_1$ and $\mathcal{R}_0 \propto \kappa$.
(2) Provide increased support for research initiatives aimed at improving the effectiveness of COVID-19 vaccines, particularly with respect to protection against infection.
(3) Ensure the availability of accessible and affordable testing centers. Increased testing enhances the ability to identify and isolate infected individuals, thereby increasing the parameters θ and θ_1.
(4) Establish isolation facilities for individuals who are unable to self-isolate, such as those who are homeless or living in overcrowded households. Under ideal conditions, isolated individuals do not contribute to the spread of infection (see Eq. (16)).

Finally, this study offers several avenues for future research. These include the identification of cost-effective intervention strategies that optimize disease control while minimizing economic burden, as well as the development of stochastic models to incorporate uncertainty in transmission dynamics and intervention effectiveness.

CRediT authorship contribution statement

Tesfalem A. Tegegn: Writing – review & editing, Writing – original draft, Formal analysis, Data curation, Conceptualization. **Yibeltal A. Terefe:** Writing – review & editing, Writing – original draft, Formal analysis, Conceptualization.

Declaration of competing interest

The authors declare that they have no known competing financial interests or personal relationships that could have appeared to influence the work reported in this paper.

Acknowledgments

The authors gratefully acknowledge the anonymous reviewers and the Associate Editor for their insightful comments and suggestions, which have significantly enhanced this work. Part of this work was presented at the workshop "On Research Trend in Mathematical Modeling and Analysis in Life Sciences" held at Tshikwalo Game Lodge, Dinokeng Game Reserve, Pretoria, South Africa and at the "Second annual One Health Symposium" held at University of Pretoria, Pretoria, South Africa. The first author acknowledges the following grants for their financial support;

DSI-NRF Center of Excellence in Mathematical and Statistical Sciences (CoE-Mass) ref. No. 2022-003-21F-trends.

SARCHI chair in Mathematical Models and Methods in Bio-engineering and Bio-sciences (M^3B^2).

Appendix A. Supplementary data

Supplementary material related to this article can be found online at https://doi.org/10.1016/j.chaos.2025.116870.

Data availability

We used open-access COVID-19 data from the Johns Hopkins University Coronavirus Resource Center (https://github.com/CSSEGISandData/COVID-19, with full citation provided in the manuscript).

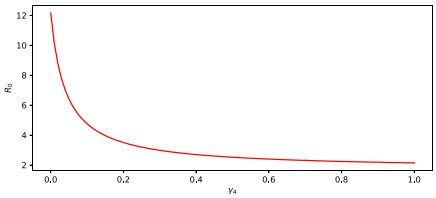

(a) Graphical visualizing the sensitivity of R_0 to γ_4

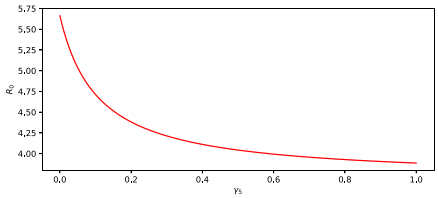

(b) Graphical visualizing the sensitivity of R_0 to γ_5

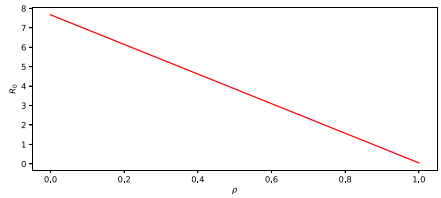

(c) Graphical visualizing the sensitivity of R_0 to ρ

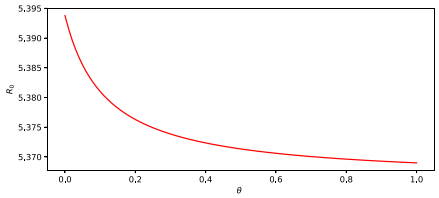

(d) Graphical visualizing the sensitivity of R_0 to θ

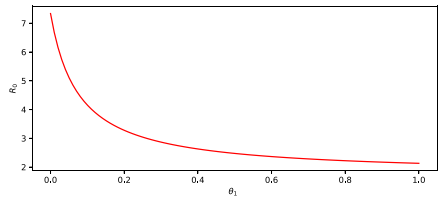

(e) Graphical visualizing the sensitivity of R_0 to θ_1

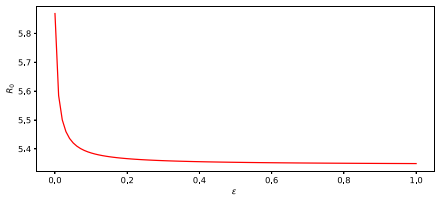

(f) Graphical visualizing the sensitivity of R_0 to ϵ

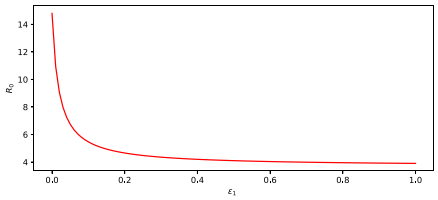

(g) Graphical visualizing the sensitivity of R_0 to ϵ_1

Fig. 10. $\mathcal{R}_0$ versus some parameters involved in Eq. (16).

References

[1] Woldometer. COVID-19 coronavirus pandemic. 2022.

[2] Atalan Abdulkadir. Is the lockdown important to prevent the COVID-19 pandemic? Effects on psychology, environment and economy-perspective. Ann Med Surg 2020;56:38–42.

[3] Ceylan Rahmiye Figen, Ozkan Burhan, Mulazimogullari Esra. Historical evidence for economic effects of COVID-19. Eur J Heal Econ 2020;21:817–23.

[4] Chaudhary Monika, Sodani PR, Das Shankar. Effect of COVID-19 on economy in India: Some reflections for policy and programme. J Heal Manag 2020;22(2):169–80.

[5] Das Kabita, Behera Rajiba Lochan, Paital Biswaranjan. Socio-economic impact of COVID-19. In: COVID-19 in the environment. Elsevier; 2022, p. 153–90.

[6] Deb Pragyan, Furceri Davide, Ostry Jonathan D, Tawk Nour. The economic effects of COVID-19 containment measures. Open Econ Rev 2022;33(1):1–32.

[7] Mou Jinjin. Research on the impact of COVID-19 on global economy. In: IOP conference series: earth and environmental science, vol. 546, IOP Publishing; 2020, 032043.

[8] Singh Kavita, Kondal Dimple, Mohan Sailesh, Jaganathan Suganthi, Deepa Mohan, Venkateshmurthy Nikhil Srinivasapura, et al. Health, psychosocial, and economic impacts of the COVID-19 pandemic on people with chronic conditions in India: a mixed methods study. BMC Public Health 2021;21:1–15.

[9] Condon Jeffrey, Kwiatkowski Lrzysztof, Singer Vivien, Smit Sven. The coronavirus effect on global economic sentiment. 2022.

[10] WHO. Corona virus. 2022.

[11] Van Doremalen Neeltje, Bushmaker Trenton, Morris Dylan H, Holbrook Myndi G, Gamble Amandine, Williamson Brandi N, et al. Aerosol and surface stability of SARS-CoV-2 as compared with SARS-CoV-1. N Engl J Med 2020;382(16):1564–7.

[12] Krämer Alexander, Kretzschmar Mirjam, Krickeberg Klaus. Modern infectious disease epidemiology: concepts, methods, mathematical models, and public health. Springer; 2010.

[13] Wu Joseph T, Leung Kathy, Leung Gabriel M. Nowcasting and forecasting the potential domestic and international spread of the 2019-nCoV outbreak originating in Wuhan, China: a modelling study. Lancet 2020;395(10225):689–97.

[14] Garba Salisu M, Lubuma Jean M-S, Tsanou Berge. Modeling the transmission dynamics of the COVID-19 pandemic in South Africa. Math Biosci 2020;328:108441.

[15] Kassa Semu M, Njagarah John BH, Terefe Yibeltal A. Analysis of the mitigation strategies for COVID-19: from mathematical modelling perspective. Chaos Solitons Fractals 2020;138:109968.

[16] Terefe YA, Njagarah JBH, Kassa SM. Effect of cross-border migration on the healthcare system of a destination community: Insights from mathematical modelling of COVID-19 in a developing country. Math Comput Simulation 2023;208:444–79.

[17] CSSEGISandData. COVID-19 data repository. 2023.

[18] Busenberg Stavros, Cooke Kenneth. Vertically transmitted diseases: models and dynamics, vol. 23, Springer Science & Business Media; 1993.

[19] Terefe Yibeltal Adane. A sex-structured model for the transmission of trichomoniasis with possible reinfection. Math Popul Stud 2021;28(2):81–103.

[20] Stuart Andrew, Humphries Anthony R. Dynamical systems and numerical analysis, vol. 2, Cambridge University Press; 1998.

[21] Chavez C Castillo, Feng Z, Huang W. On the computation of $\mathcal{R}_0$ and its role on global stability. In: Mathematical approaches for emerging and re-emerging infection diseases: an introduction, vol. 125, 2002, p. 31–65.
[22] Diekmann Odo, Heesterbeek Johan Andre Peter. Mathematical epidemiology of infectious diseases: model building, analysis and interpretation, vol. 5, John Wiley & Sons; 2000.
[23] van den Driessche P, Watmough James. Further notes on the basic reproduction number. In: Mathematical epidemiology. 2008.
[24] Shuai Zhisheng, Heesterbeek JAP, van Den Driessche P. Extending the type reproduction number to infectious disease control targeting contacts between types. J Math Biol 2013;67:1067–82.
[25] Castillo-Chavez Carlos, Song Baojun. Dynamical models of tuberculosis and their applications. Math Biosci Eng 2004;1(2):361–404.
[26] La Salle Joseph P. The stability of dynamical systems. SIAM; 1976.
[27] Rubin Rita. COVID-19 vaccines vs variants—determining how much immunity is enough. Jama 2021;325(13):1241–3.
[28] Andrews Nick, Stowe Julia, Kirsebom Freja, Toffa Samuel, Rickeard Tim, Gallagher Eileen, et al. COVID-19 vaccine effectiveness against the omicron (b. 1.1. 529) variant. N Engl J Med 2022;386(16):1532–46.
[29] Chung Hannah, He Siyi, Nasreen Sharifa, Sundaram Maria E, Buchan Sarah A, Wilson Sarah E, et al. Effectiveness of BNT162b2 and mRNA-1273 COVID-19 vaccines against symptomatic SARS-CoV-2 infection and severe COVID-19 outcomes in Ontario, Canada: test negative design study. Bmj 2021;374.
[30] Chen Kaijing, Wei Fengying, Zhang Xinyan, Jin Hao, Zhou Ruiyang, Zuo Yue, et al. Dynamics of an SVEIR transmission model with protection awareness and two strains. Infect Dis Model 2025;10(1):207–28.
[31] World Bank. Population growth (annual %). 2022.
[32] CDC. Impact of vaccination on risk of COVID-19–related mortality. 2022.
[33] Mengstu Selamawit, Berha Alemseged Beyene. Safety and efficacy of COVID-19 vaccine in Africa: Systematic review. Infect Drug Resist 2023;3085–100.
[34] Benisek Alexandra, DerSarkissian Carol. COVID vaccines compared. 2022.
[35] Sadoff Jerald, Gray Glenda, Vandebosch An, Cárdenas Vicky, Shukarev Georgi, Grinsztejn Beatriz, et al. Safety and efficacy of single-dose Ad26. COV2. S vaccine against COVID-19. N Engl J Med 2021;384(23):2187–201.
[36] Soheili Marzieh, Khateri Sorour, Moradpour Farhad, Mohammadzedeh Pardis, Zareie Mostafa, Mortazavi Seyede Maryam Mahdavi, et al. The efficacy and effectiveness of COVID-19 vaccines around the world: a mini-review and meta-analysis. Ann Clin Microbiol Antimicrob 2023;22(1):42.
[37] Jeong Minseo, Pike Harriet. Sinovac COVID-19 vaccine: What are the side effects? 2022.
[38] Paleker M, Tembo YA, Davies MA, Mahomed H, Pienaar D, Madhi SA, et al. Asymptomatic COVID-19 in South Africa–implications for the control of transmission. Public Heal Action 2021;11(2):58–60.
[39] Alexandra, Benisek. Coronavirus recovery. 2023.
[40] Bai Yan, Yao Lingsheng, Wei Tao, Tian Fei, Jin Dong-Yan, Chen Li-juan, et al. Presumed asymptomatic carrier transmission of COVID-19. Jama 2020;323(14):1406–7.
[41] Puckey Melisa. How do COVID-19 symptoms progress and what causes death. In: Drugs. com, vol. 64, 2022, https://www.drugs.com/medical-answers/covid-19-symptoms-progress-death-35362.
[42] Walsh Kieran A, Jordan Karen, Clyne Barbara, Rohde Daniela, Drummond Linda, Byrne Paula, et al. SARS-CoV-2 detection, viral load and infectivity over the course of an infection. J Infect 2020;81(3):357–71.
[43] Zhou Fei, Yu Ting, Du Ronghui, Fan Guohui, Liu Ying, Liu Zhibo, et al. Clinical course and risk factors for mortality of adult inpatients with covid-19 in Wuhan, China: a retrospective cohort study. Lancet 2020;395(10229):1054–62.
[44] Tegally Houriiyah, Wilkinson Eduan, Giovanetti Marta, Iranzadeh Arash, Fonseca Vagner, Giandhari Jennifer, et al. Detection of a SARS-CoV-2 variant of concern in South Africa. Nature 2021;592(7854):438–43.
[45] NCIRD. COVID-19 vaccine effectiveness. 2024.
[46] Martcheva Maia. An introduction to mathematical epidemiology, vol. 61, Springer; 2015.
[47] Terefe YA, Gaff H, Kamga Morgan, van der Mescht Luther. Mathematics of a model for Zika transmission dynamics. Theory Biosci 2018;137:209–18.
[48] Wajnberg Ania, Amanat Fatima, Firpo Adolfo, Altman Deena R, Bailey Mark J, Mansour Mayce, et al. Robust neutralizing antibodies to SARS-CoV-2 infection persist for months. Science 2020;370(6521):1227–30.
[49] WHO. Vaccine efficacy, effectiveness and protection. 2022.